

UniF²ace: Fine-grained Face Understanding and Generation with Unified Multimodal Models

Junzhe Li^{1,2}, Xuerui Qiu³, Linrui Xu⁴, Liya Guo⁵, Delin Qu⁶
Tingting Long², Chun Fan², Ming Li⁷

¹School of Computer Science, Peking University ²Computer Center, Peking University

³Institute of Automation, Chinese Academy of Sciences ⁴Central South University

⁵Yau Mathematical Sciences Center and Department of Mathematical Sciences, Tsinghua University

⁶Fudan University ⁷Guangdong Laboratory of Artificial Intelligence and Digital Economy (SZ)

lijunzhe1028@stu.pku.edu.cn, {l.tingting, fanchun}@pku.edu.cn, qiuxuerui2024@ia.ac.cn
xulinrui@csu.edu.cn, gly22@mails.tsinghua.edu.cn, dlqu22@m.fudan.edu.cn, ming.li@u.nus.edu

Abstract

Unified multimodal models (UMMs) have emerged as a powerful paradigm in foundational computer vision research, demonstrating significant potential in both image understanding and generation. However, existing research in the face domain primarily focuses on coarse facial attribute understanding, with limited capacity to handle fine-grained facial attributes and without addressing generation capabilities. To overcome these limitations, we propose UniF²ace, the first UMM tailored specifically for fine-grained face understanding and generation. In general, we train UniF²ace on a self-constructed, specialized dataset utilizing two mutually beneficial diffusion techniques and a two-level mixture-of-experts architecture. Specifically, we first build a large-scale facial dataset, UniF²ace-130K, which contains 130K image-text pairs with one million question-answering pairs that span a wide range of facial attributes. Second, we establish a theoretical connection between discrete diffusion score matching and masked generative models, optimizing both evidence lower bounds simultaneously, which significantly improves the model’s ability to synthesize facial details. Finally, we introduce both token-level and sequence-level mixture-of-experts, enabling efficient fine-grained representation learning for both understanding and generation tasks. Extensive experiments on UniF²ace-130K demonstrate that UniF²ace outperforms existing UMMs and generative models, achieving superior performance across both understanding and generation tasks.

1. Introduction

Recently, unified multimodal models (UMMs) have emerged as a thriving and vibrant research field in mul-

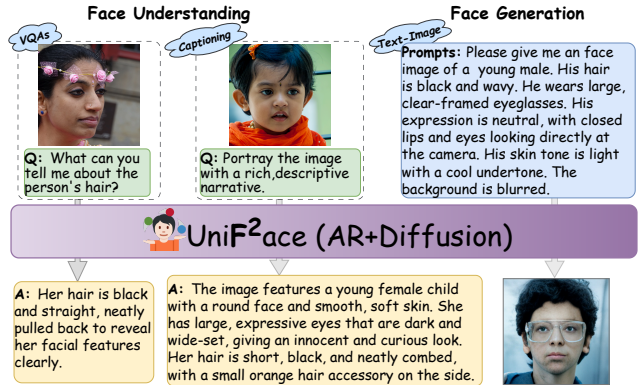


Figure 1. UniF²ace is the first unified multimodal model specifically designed for face understanding and generation, encompassing tasks such as visual question answering, face image captioning and text-to-face image generation. The generated responses and images demonstrate UniF²ace’s significant potential in capturing fine-grained face attributes.

timodal learning community, enabling both image understanding and generation within a single network. This any-to-any generation approach marks a significant step toward artificial general intelligence (AGI) [23, 49, 63]. UMMs enhance the flexibility and scalability of multimodal systems, streamlining the handling of diverse tasks and laying the foundation for more generalized systems that contribute to the development of world models [2, 26, 36, 54, 67, 69, 77].

Fine-grained face understanding and generation are essential for advancing computer vision and AGI, given the central role of faces in daily life. For example, accurate face understanding enables applications such as identity verification [51], emotion recognition [15, 46], and human-computer interaction [9, 33]. High-fidelity face generation drives progress in creative industries [37], vir-

tual avatars [71], and data augmentation for model robustness [38]. These tasks also push the boundaries of multimodal reasoning and generative modeling, advancing AI’s ability to capture human-like details, thereby bridging the gap between AI and human perception.

Recent works in the face domain have addressed understanding and generation as separate tasks, each with inherent limitations. For face understanding, the investigators typically fine-tune pretrained multimodal large language models (MLLMs) on facial image-text datasets [8, 52, 68, 70, 72]. For instance, Face-MLLM [52] re-annotates the LAION-Face dataset [76] using Gemini-1.5-pro [55] and fine-tunes LLaVA-v1.5 [31] for face understanding. However, studies [24, 52] reveal that general-purpose MLLMs, such as the LLaVA family, struggle with fine-grained facial attribute understanding, leading to low-quality captions and inaccurate visual question-answering (VQA) pairs. Meanwhile, face generation methods [16, 20, 21, 41] primarily rely on diffusion models conditioned on multimodal inputs, such as semantic masks [61] and sketches [12, 60]. For example, Face-Makeup [11] conditions face generation on an input face image and a text prompt to synthesize customized images while preserving structural integrity. However, these methods heavily depend on predefined visual prompts, limiting the model’s ability to extract fine-grained facial details from textual descriptions. Additional related works of unified multimodal models and face multimodal models can be found in **Appendix A**.

In this work, we propose UniF²ace (see Fig. 1), the first UMM for the face domain, designed to simultaneously perform face understanding and generation tasks while capturing fine-grained facial attributes from both image and text modalities. The key challenges include aligning coarse captions with detailed facial attributes, achieving uniform embedding of images and text for seamless cross-modal alignment, and learning fine-grained facial representations for both understanding (image-to-text) and generation (text-to-image). To support our research, we first introduce UniF²ace-130K, a dataset containing 130K facial image-text pairs and one million visual question-answering (VQA) pairs, spanning 46 attributes related to appearance, actions, and emotions. We annotate facial attributes for a large set of images using our trained classifiers on the high-quality CelebV-HQ dataset [78]. These attributes correct and enhance captions generated by general MLLMs like GPT-4o [17], yielding precise fine-grained facial descriptions. Using carefully crafted prompts, we employ GPT-4 [1] to generate diverse VQAs, *i.e.*, detailed description, conversation about face attributes, reasoning about action, based on these enhanced captions.

For cross-modal alignment within a single network, we combine autoregressive models for understanding and diffusion models for generation, inspired by Show-o [67]. We

argue that synthesizing facial attributes consistent with text descriptions is more challenging than face understanding. To address this, we bridge two typical discrete diffusion paradigms, *i.e.*, masked generative models [5] and score-based diffusion models [39], through theoretical proof, enabling simultaneous optimization of evidence lower bounds (ELBOs) and significantly improving generation quality. Finally, to learn fine-grained patterns for both image-to-text understanding and text-to-image generation, we introduce a powerful and efficient network architecture with token-level and sequence-level mixture-of-experts (MoE) layers, enabling adaptive handling of diverse attributes. We evaluate UniF²ace on the UniF²ace-130K test dataset, comparing its performance with state-of-the-art (SOTA) UMMs, *e.g.*, JanusFlow [36] and TokenFlow [44]. Additionally, we compare it against advanced generative models, *e.g.*, LlamaGen [53], Stable Diffusion 3 [14] and understanding-only multimodal models *e.g.*, Qwen2-VL [59], InternVL2.5 [7] using popular metrics. The results demonstrate that UniF²ace significantly outperforms models of similar parameter scales and achieves performance comparable to, or even surpassing, larger-scale models.

Our main contributions in this work are as follows:

- We introduce UniF²ace, the first unified multimodal model for fine-grained face understanding and generation, establishing a solid baseline for future research.
- We present UniF²ace-130K, a dataset containing 130K fine-grained image-caption pairs and one million VQAs. We develop an automated pipeline for generating fine-grained multimodal datasets, leveraging face attribute classifiers to enhance and correct captions generated by MLLMs.
- We establish a theoretical connection by integrating score matching into the masked generative model, enabling the simultaneous optimization of two maximum likelihood ELBOs and benefiting the face generation. Additionally, we explore a hybrid MoE architecture at both token and sequence levels to improve fine-grained representation learning for both understanding and generation tasks.

2. Fine-grained Facial Dataset

To overcome the limitations of existing datasets in the realm of multimodal facial modeling, we introduce a high-quality dataset called *UniF²ace-130K*, which boasts a remarkable alignment between facial images and textual descriptions (see Fig. 2). This dataset encompasses nearly 130K facial images, each paired with richly detailed captions. Additionally, it contains approximately 1M visual question answers, significantly enhancing its value for training and evaluating multimodal models. By offering such a comprehensive resource, we aim to propel advancements in facial image understanding and generation, establishing a solid foundation

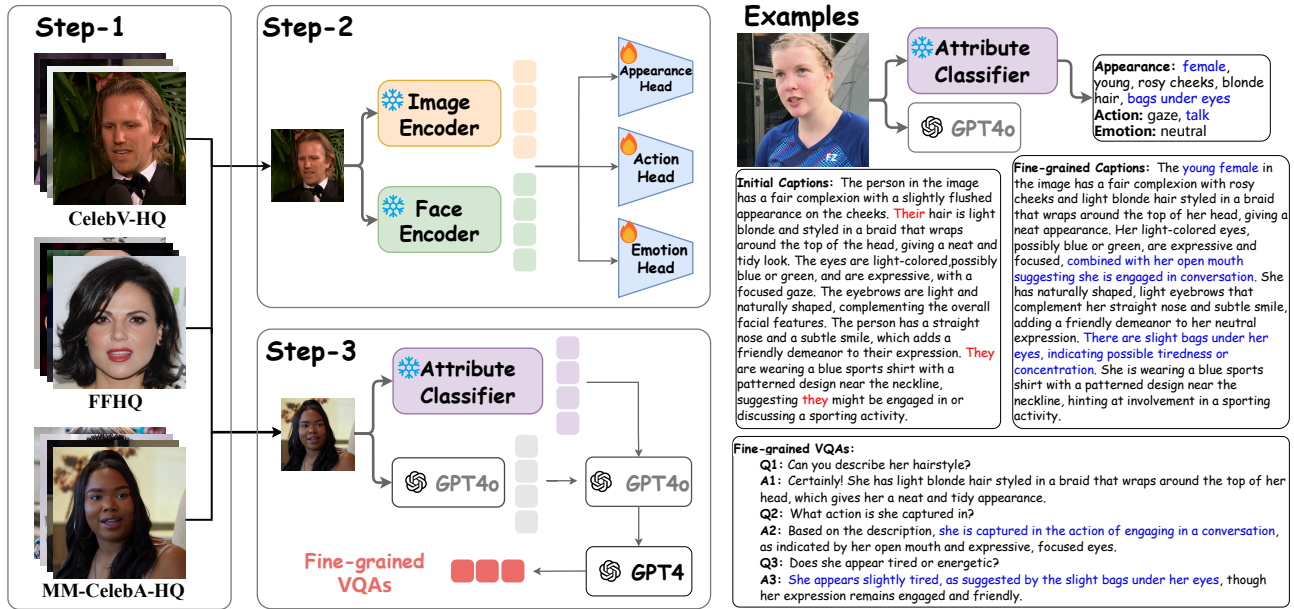


Figure 2. Pipeline and examples of UniF²ace-130K construction. Left: A three-stage pipeline for building UniF²ace-130K. Step-1: High-quality face images are collected. Step-2: Detailed captions are generated by GPT-4o with a face attribute model trained to classify fine-grained appearance, action, and emotion. Step-3: Question-answering pairs are created. These stages collectively refine GPT-4o-generated captions and produce fine-grained descriptions for VQAs generation. Right: A representative example showcasing UniF²ace-130K’s ability to correct (e.g., gender), enhance (e.g., bags under eyes), and reason (e.g., talking, slight tiredness) in GPT-4o-generated captions.

for a wide range of multimodal learning tasks. The creation of UniF²ace-130K encompassed three key stages. **(1) Step-1:** Collect high-quality facial images. **(2) Step-2:** Generate detailed captions. **(3) Step-3:** Create question-answering pairs. Each stage is outlined in detail below.

(1) Step-1: Collect High-quality Facial Images. In this step, we curated more than 130,000 high-quality facial images from the following distinguished datasets. CelebV-HQ [78] is a large-scale video dataset featuring 35,666 clips representing 15,653 identities, each clip meticulously annotated with 83 facial attributes. We extracted one key frames from each video to utilize detailed annotations for fine-grained face-text alignment. Flickr-Faces-HQ (FFHQ) [19] provided 70,000 high-quality PNG images at a resolution of 1024 by 1024, offering substantial diversity in attributes such as age and ethnicity. Multi-Modal-CelebA-HQ (MM-CelebA-HQ) [66] contributed 30,000 high-resolution images paired with descriptive captions that have proven invaluable for facial generation and analysis.

(2) Step-2: Generate Detailed Captions. Existing face image datasets often lack detailed descriptions of fine-grained attributes like bags under eyes or jewelry. To handle this, we develop a two-stage caption generation process.

In Stage I, we employed an advanced MLLM such as GPT-4o [17] to produce initial captions. We designed a specialized prompt that incorporated brief face descriptions from the MM-CelebA-HQ dataset [66] to help GPT-4o

accurately describe key facial attributes including appearance, emotion, and actions. The detailed descriptions of all prompts are presented later (see the Figure 4 of the supplementary material *i.e.*, Fig.S4).

In Stage II, we refined these captions by training face attribute classification models using the CelebV-HQ dataset [78]. Focusing on single-person images, we used the pre-trained face model AntelopeV2¹ to extract face embeddings. By combining these with image embeddings from CLIP [45], we trained classification heads for appearance, action, and emotion attributes. We selected 29 appearances with accuracies over 93%, 10 actions with accuracies over 87%, and 7 emotions with accuracies over 80% as final predictions for inference. These highly accurate attributes were then predicted for all remaining images in FFHQ and MM-CelebA-HQ datasets [19, 66]. Finally, a prompt integrating these classification results with the Stage I captions was fed into GPT-4o to generate final captions that are both highly accurate and diverse.

(3) Step-3: Create Question-answering Pairs. In this step, we proposed 1M VQAs covering diverse facial appearances, emotions, and character action reasoning for our UniF²ace-130K dataset. These VQAs are designed to enhance MLLMs’ ability to understand fine-grained facial attributes through instruction tuning. Inspired by LLaVA [32], we carefully designed prompts to enable GPT-

¹<https://github.com/deepinsight/insightface>

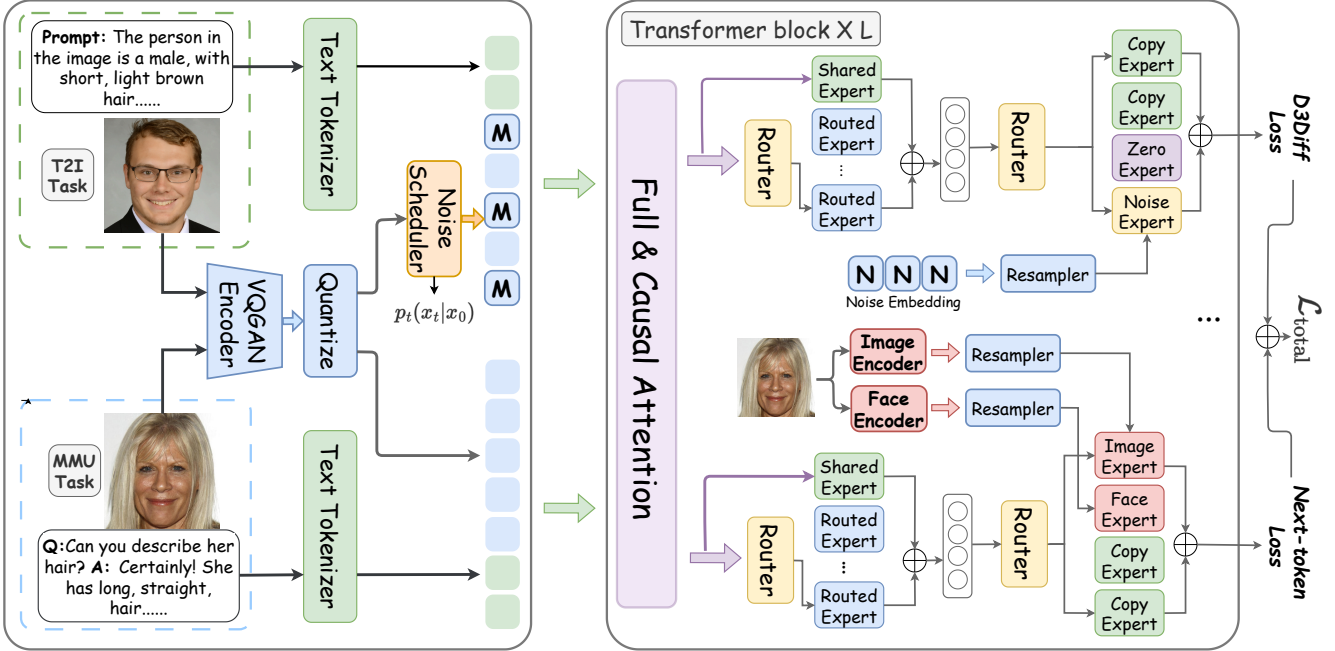


Figure 3. Our UniF²ace architecture integrates Text-to-Image (T2I) and Multimodal Understanding (MMU) tasks. Text inputs are encoded via a tokenizer, while input images are processed through a VQGAN encoder, merging into a unified token sequence. A noise scheduler masks a subset of image tokens, which are then processed by a Transformer with Mixture-of-Experts (MoE) layers. These MoE layers are grouped for generation and understanding tasks, with the first operating at the token level using shared and routed experts, and the second incorporating domain-specific features at the sequence level. This hierarchical design enables fine-grained facial feature processing. The noise scheduler outputs $p_t(x_t|x_0)$ for D3Diff loss computation, combined with text autoregressive loss to form the training objective.

4 [1] to generate a series of VQAs based on image captions, facilitating fine-grained understanding and reasoning. Most current face-text datasets lack VQAs, while VQAs in general image-text datasets often focus on people’s clothing, location, and behavior, neglecting detailed facial descriptions. In contrast, our proposed VQAs encompass diverse facial details, including hair, nose, eyes, mouth, ears, skin, eyebrows, and adornments. Additionally, since facial attributes can reflect a character’s ongoing actions, our VQAs incorporate detailed reasoning processes to infer and describe these actions. By organizing the VQAs into the same format as the LLaVA dataset [32], we streamlined the process of adapting multimodal face models for post-training. This alignment minimizes alteration costs, ensuring efficient integration and enabling the models to leverage both datasets seamlessly for improved performance.

3. UniF²ace

We introduce a unified multimodal model, UniF²ace, designed to seamlessly model both the understanding and generation of fine-grained facial attributes. Our approach is realized from two perspectives: generation strategy (Section 3.1) and network architecture (Section 3.2). Regarding the generation strategy, we recognize that the generation of fine-grained facial attributes is significantly more challenging than understanding tasks, as highlighted in prior stud-

ies [13, 67, 77]. To address this, we harness the theory of score matching in discrete diffusion [35] and propose the dual discrete diffusion (D3Diff) training strategy, ensuring the meticulous synthesis of facial details. On the network architecture front, existing UMMs [67, 77] typically employ dense architectures and demand extensive training data. To overcome these limitations, we introduce token-level and sequence-level Mixture-of-Experts (MoE) layers. Distinct MoE modules are designed for generation and comprehension tasks, selectively integrating information such as facial embeddings to enhance the model’s ability to capture subtle facial attributes.

3.1. Dual Discrete Diffusion

In this section, we first introduce the discrete diffusion model, then explain the masked generative model and its variants, and finally combine the masked generative model with the score matching method to achieve stable optimization of the generative model.

In the discrete diffusion process, each token is confined to a finite set, $\mathcal{X} = \{1, \dots, N\}$, so its probability at time t is represented as a vector $p_t \in \mathbb{R}^N$. The forward process is modeled as a continuous-time Markov chain (CTMC) governed by the linear ordinary differential equation (ODE):

$$\frac{d}{dt} p_{t|s}(y | x) = p_{t|s}(y | x) Q_t, \quad (1)$$

with the initial condition $p_0 \approx p_{\text{data}}$ and the distribution converging to $p_{\text{stationary}}$ as $t \rightarrow \infty$. Here, \mathbf{Q}_t represents a time-dependent sequence of transition matrices. The solution to this ODE is expressed as:

$$\mathbf{P}_{t|s} = \exp((\bar{\sigma}(t) - \bar{\sigma}(s)) \mathbf{Q}), \quad (2)$$

where $\bar{\sigma}(t) = \int_0^t \sigma(s) ds$ denotes the cumulative noise level and \exp denotes the matrix exponential. Following [34], the reverse process is formalized as:

$$\frac{dp_{T-t}}{dt} = \tilde{\mathbf{Q}}_{T-t} p_{T-t}, \quad \tilde{\mathbf{Q}} = \frac{p_t(y)}{p_t(x)} \mathbf{Q}_t(x, y), \quad (3)$$

The score-based discrete diffusion model [34] introduces a training-stable loss $\mathcal{L}_{\text{score}}(s_\theta)$ that models the denoising process by estimating the score. This is defined as follows:

$$\mathbb{E}_{x \sim p} \left[\sum_{y \neq x} w_{xy} \left(s_\theta(x)_y - \frac{p(y)}{p(x)} \log s_\theta(x)_y + K \left(\frac{p(y)}{p(x)} \right) \right) \right], \quad (4)$$

where $s_\theta(x_t, t) \approx \left[\frac{p_t(y_t)}{p_t(x_t)} \right]_{y_t \in \mathcal{X}}$ is the predicted score from the neural network, and $K(a) = a(\log a - 1)$ is a normalizing constant ensuring $\mathcal{L}_{\text{score}} \geq 0$.

In our work, we focus on the absorbing state, namely the masked state, which is commonly used in masked generative models [5, 67]. We assume independence between tokens, as supported by [4, 47, 48]; the exact formulation is provided in **Appendix C**. A key insight is that within masked generative models the posterior probability $p_\theta(x_0 | x_t)$ can be linked to the score in a discrete diffusion model using Bayes' theorem:

$$p_\theta(x_0 | x_t) \approx p_t(x_t | x_0) \frac{p_t(x_0)}{p_t(x_t)} = p_t(x_t | x_0) s_\theta(x_t), \quad (5)$$

Leveraging this connection, we propose a novel loss, the dual discrete diffusion (D3Diff) loss, for the posterior probability network, which is based on explicitly defined stochastic differential equations (SDEs) and is formulated as follows:

$$\mathcal{L}_{\text{D3Diff}} = \sum_{t=1}^T \mathbb{E}_{q(\mathbf{x}_0)q(\mathbf{x}_t|\mathbf{x}_0)} [\log p_\theta(\mathbf{x}_0|\mathbf{x}_t)] + \alpha \mathcal{L}_{\text{score}}(p_t(\mathbf{x}_t|\mathbf{x}_0) p_\theta(\mathbf{x}_0|\mathbf{x}_t)), \quad (6)$$

Here, $q(\mathbf{x}_0)$ represents the data distribution, $q(\mathbf{x}_t|\mathbf{x}_0)$ and $p_t(\mathbf{x}_t|\mathbf{x}_0)$ are forward diffusion probabilities, and $p_\theta(\mathbf{x}_0|\mathbf{x}_t)$ is the network-predicted posterior with parameters θ . The score loss $\mathcal{L}_{\text{score}}$ is balanced by hyperparameter α . Equation 6 links masked generative models and score-based models in the discrete domain via Bayes' theorem, enabling score loss application on pre-trained unified multimodal models [67] without additional cost. Unlike traditional masked generative loss, which relies solely on likelihood, our D3Diff loss optimizes two distinct upper bounds

of maximum likelihood. In **Appendix D**, we prove that our score loss provides a tighter upper bound on the negative log-likelihood of the original data compared to the conventional masked generative loss.

3.2. Multi-level Grouped Mixture-of-Expert

To capture fine-grained facial attributes while maintaining hardware-friendly facial embeddings, we design distinct MoE layers, termed Multi-level Grouped MoE, tailored for both generation and understanding subtasks. This ensures optimal performance for each task, as illustrated in Fig. 3. We incorporate a sequence-level MoE layer after the token-level MoE layer to effectively process instance-level inputs, such as images and facial embeddings.

Token-Level MoE. Following DeepSeekMoE [10], we partition a feedforward neural network (FFN) into multiple experts with reduced hidden dimensions and use a Top-K activation strategy (Fig. 3). We also employ shared experts to integrate generalized knowledge across contexts. Unlike prior methods, we introduce grouped MoE, dividing experts into two groups based on the different tasks of Text-to-Image (T2I) and Multimodal Understanding (MMU). Each group combines shared and routed MoE, with expert-level balance loss computed independently per group:

$$\mathcal{L}_{\text{Balance}} = \lambda_{\text{T2I}} \sum_{i=1}^{N_{\text{T2I}}} f_i P_i + \lambda_{\text{MMU}} \sum_{j=1}^{N_{\text{MMU}}} f_j P_j, \quad (7)$$

where λ_{T2I} and λ_{MMU} are balance factors; N_{T2I} and N_{MMU} means routed experts for T2I and MMU tasks, respectively; f and P denote expert selection frequency and probability.

Sequence-Level MoE. We propose sequence-level MoE, where distinct experts process the entire image feature. We design three experts for the T2I group: copy expert (skip operation), zero expert (discard operation), and noise expert. Following MOE++ [18], the copy and zero experts require no additional parameters.

$$\mathbf{E}_{\text{copy}}(\mathbf{x}) = \mathbf{x} \quad \text{and} \quad \mathbf{E}_{\text{zero}}(\mathbf{x}) = 0, \quad (8)$$

where $\mathbf{E}_{\text{copy}}(\cdot)$ is the copy expert and $\mathbf{E}_{\text{zero}}(\cdot)$ is the zero expert. For the noise expert $\mathbf{E}_{\text{noise}}(\cdot)$, we first integrate the time-step embedding, which operates on the noise level $\bar{\sigma}(t)$ to obtain the noise embedding vector $\mathbf{v}_{\text{noise}}$, following score-based discrete diffusion models [34]. Then, a resampler $\mathcal{S} : \mathbb{R}^h \rightarrow \mathbb{R}^{L \times D}$ maps $\mathbf{v}_{\text{noise}}$ into the sequence feature space (see **Appendix E** for resampler details). The resampled noise embedding is added as a matrix to the sequence feature. Formally, the noise expert's output is:

$$\mathbf{E}_{\text{noise}}(\mathbf{x}) = \lambda_1 \mathbf{x} + \lambda_2 \mathcal{S}(\mathbf{v}_{\text{noise}}), \quad (9)$$

and $[\lambda_1, \lambda_2]$ is calculated by:

$$[\lambda_1, \lambda_2] = \text{Softmax}(\mathbf{W}_{\text{noise}} \cdot \text{Flatten}(\mathbf{x})), \quad (10)$$



"A young female child with a **round face**, wearing a playful **green hat with monster-like features including white eyes**. Her long hair peeks out from under the hat. The child's **cheeks are rosy**, and her **lips are slightly parted**. She has **light-colored eyes**, giving an expression of **curiosity or wonder**. Dressed in a **bright red jacket**, she adds a vibrant contrast to the scene. The background is a **softly blurred outdoor winter setting**."



"The image features a female with **long, straight black hair**. She has a fair complexion with a smooth skin texture and **well-defined, arched eyebrows** that complement her **deep-set, dark brown eyes**. Her nose is pointy and she has **full lips with a natural, subtle color**. The person is **wearing hoop earrings** and smiling or laughing conveying a sense of happiness, with **an overall expression that is calm and composed**."

Figure 4. Comparative analysis of face images generation quality across SDXL [43], TokenFlow [44], OmniFlow [23], Show-o [67], and UniF²ace. Our proposed UniF²ace effectively captures more detailed information from prompts. We highlight fine-grained attributes.

where $\mathbf{W}_{\text{noise}} \in \mathbb{R}^{2 \times (L \cdot D)}$ is a trainable weight matrix. In the MMU task, we include copy experts and introduce CLIP experts and face experts, which are similar to noise experts. Next we extract image embeddings by CLIP [45] and face embeddings using AntelopeV2 as supplementary features to enhance fine-grained facial attribute capture. Formally, the outputs of the CLIP and face experts are:

$$\mathbf{E}_{\text{CLIP}}(\mathbf{x}) = \alpha_1 \mathbf{x} + \alpha_2 \mathcal{S}(\mathcal{G}(\mathbf{X})), \quad (11)$$

$$\mathbf{E}_{\text{face}}(\mathbf{x}) = \alpha_1 \mathbf{x} + \alpha_2 \mathcal{S}(\mathcal{F}(\mathbf{X})), \quad (12)$$

where \mathcal{G} and \mathcal{F} are the image encoder and face encoder, respectively. \mathbf{X} is the input face image.

3.3. Overall Training Objectives

To perform both auto-regressive and discrete score-based diffusion modeling, we employ two learning objectives: 1) Next Token Prediction (NTP) and 2) Dual Discrete Diffusion. Given a sequence with N image tokens $\mathcal{X} = \{\mathbf{X}_1, \mathbf{X}_2, \dots, \mathbf{X}_N\}$ and M text tokens $\mathcal{Y} = \{\mathbf{Y}_1, \mathbf{Y}_2, \dots, \mathbf{Y}_M\}$. Then we maximize the likelihood of text tokens \mathcal{Y} by employing the standard language modeling objective (NTP loss):

$$\mathcal{L}_{\text{MMU}} = \sum_{i=1}^M \log P(\mathbf{Y}_i | \mathbf{Y}_{<i}, \mathcal{X}), \quad (13)$$

Next, the overall training objectives of UniF²ace are formulated as:

$$\mathcal{L}_{\text{total}} = \mathcal{L}_{\text{MMU}} + \lambda \mathcal{L}_{\text{D3Diff}}, \quad (14)$$

where λ denotes a balancing coefficient, which is set to 1 in our experiments.

4. Experiment

4.1. Implementation

We train our model on the UniF²ace-130K training dataset part, comprising 120K 256×256 face images, each annotated with detailed captions and seven to eight VQAs, about 900K. And more details about implementations can be found in **Appendix B**. We evaluate the generation and understanding tasks separately on the UniF²ace-130K test dataset. For generation, we use VQAScore to measure the relevance of generated images to captions, reporting results based on CLIP-FlanT5-11B (VQAScore-CF5) [?] and LLaVA-v1.5-13B (VQAScore-LV) [32] for robust assessment. We also employ Fréchet Inception Distance (FID) to measure similarity to ground truth and VLM-score to evaluate facial realism. For understanding, we follow LLaVA [30] and use GPT-4o [17] and DeepSeek-v3 [29] to score responses on a 1-10 scale across two dimensions: detailed captioning (Desc-GPT, Desc-DS), assessing accuracy in capturing face attributes, and visual question answering (Conv-GPT, Conv-DS), measuring precision in responding to fine-grained queries.

4.2. Face Generation

To verify the effectiveness of UniF²ace, we compare it with SOTA generative models including autoregressive models like LlamaGen [73] and diffusion-based models like Stable

Type	Model	Method	# Params	VQAscore-CF5 \uparrow	VQAscore-LV \uparrow	FID \downarrow	VLM-score \uparrow
Gen. Only	LlamaGen [53]	AR	0.8B	0.746	0.551	183.466	49.773
	DALL-E 3 [3]	AR	-	0.845	0.644	106.477	50.122
	SD3 [14]	Diff	2B	0.903	0.671	93.471	75.944
	SDXL [43]	Diff	2.6B	0.876	0.660	123.095	72.764
Und. and Gen.	TokenFlow [44]	AR	7B	0.871	0.664	98.194	73.177
	OmniFlow [23]	Diff	3.4B	0.798	0.585	180.933	24.96
	JanusFlow [36]	AR + Diff	1.3B	0.881	0.653	72.825	61.593
	Show-o [67]	AR + Diff	1.3B	0.855	0.650	142.557	75.618
	UniF ² ace(Ours)	AR + Diff	1.8B	<u>0.894</u>	0.679	66.005	88.049

Table 1. Comparing the generative capability of UniF²ace with other generative and unified multimodal models, UniF²ace achieves state-of-the-art performance for models of the same parameter size and delivers comparable or superior results against larger models. **Bold** indicates the best performance overall, while underlined denotes the best among Und. and Gen. types. We use red to highlight the larger model size than ours.

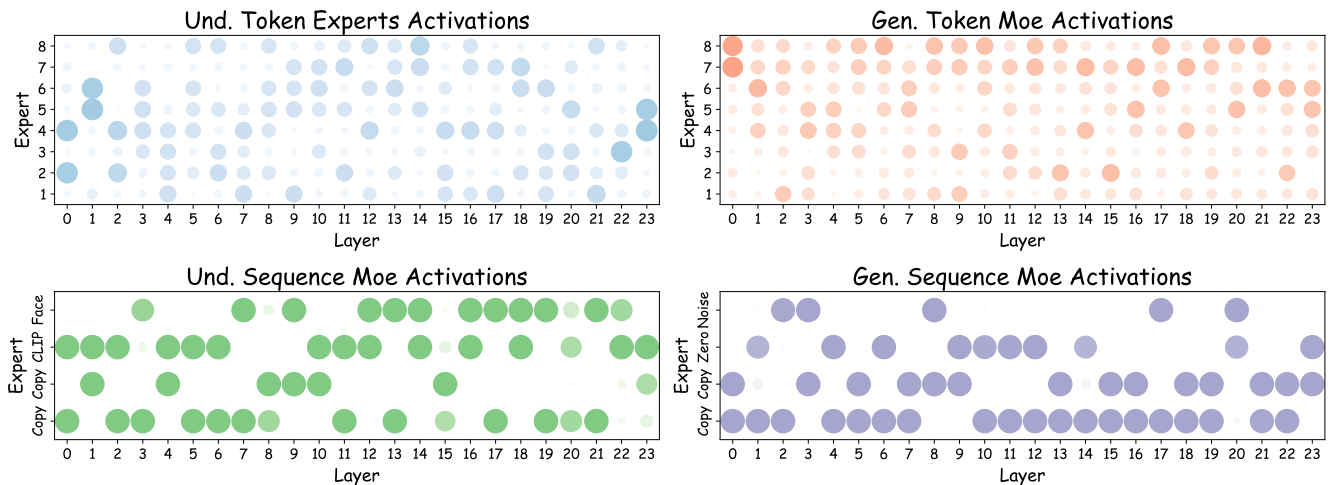


Figure 5. Activation frequency of Token-Level and Sequence-Level MoE in different layers. The left column corresponds to understanding tasks, while the right column corresponds to generation tasks. Larger circles indicate experts that are activated more frequently.

Diffusion (SD3) [14]. Additionally, we evaluate it against unified multimodal models (UMMs) using various methods including TokenFlow [44], OmniFlow [23] and others. The complete results are presented in Tab. 1. The results show that UniF²ace achieves SOTA on VQA-score-LV, FID, and VLM-score, and outperforms UMMs while nearing SD3 on VQA-score-CF5. This indicates that UniF²ace can generate higher-quality, more realistic face images while better capturing fine-grained facial attributes from text.

We conduct qualitative assessments on challenging UniF²ace-130K test scenarios involving complex facial details (see Fig. 4). The results show that UniF²ace effectively captures detailed prompts like “rosy cheeks” and “monster-like hat including white eye” in case1, and “hoop earrings” in case2. Additionally, UniF²ace generates notably more realistic face images compared to other models. More examples can be found in Fig.S1 and Fig.S2. We analyze MoE activation frequencies across layers, as shown in the right column of Fig. 5. For token-level MoEs, high activation frequencies are concentrated between experts 5 and 8,

indicating limited token feature variability in the generation task. For sequence-level MoEs, noise and zero expert activations are evenly distributed, indicating effective training with selective noise embedding and truncation.

4.3. Face Understanding

We compare UniF²ace with advanced autoregressive multimodal models like Qwen2-VL [59] and similar UMMs [65, 67]. As shown in Tab. 2, UniF²ace outperforms existing models in facial image captioning and VQA tasks with significantly fewer parameters.

We present representative cases for VQAs. As shown in Fig. 6, in case 1, compared to VILA1.5 and JanusFlow, UniF²ace focuses on more details, like “sideburns” achieving the highest score. In case 2, UniF²ace identifies subtle earrings and associates them with a stylish appearance, demonstrating its fine-grained face understanding. We also provide examples for captioning later (see Fig.S3). For MoEs in the understanding group, we analyze expert activation frequencies, as shown in the left column of Fig. 5. For token-level MoEs, tokens often select the same expert

Type	Model	Method	# Params	Desc-GPT \uparrow	Conv-GPT \uparrow	Desc-DS \uparrow	Conv-DS \uparrow
Und. Only	VILA1.5 [28]	AR	3B	4.76	5.20	6.56	6.54
	Qwen2-VL [59]	AR	7B	5.16	6.27	5.50	6.86
	LLaVA-v1.5 [31]	AR	7B	4.28	5.48	4.84	6.20
	InternVL2.5 [7]	AR	8B	5.62	5.89	6.30	6.55
Und. and Gen.	TokenFlow [44]	AR	7B	5.02	5.80	5.82	6.39
	OmniFlow [23]	Diff	3.4B	1.62	-	1.90	-
	JanusFlow [36]	AR + Diff	1.3B	4.88	6.06	5.42	6.77
	Show-o [67]	AR + Diff	1.3B	3.88	4.17	5.24	4.90
	UniF ² ace(Ours)	AR + Diff	1.8B	6.02	6.53	7.38	7.29

Table 2. Evaluation on face understanding tasks compared with advanced multimodal models and unified multimodal models. Our UniF²ace achieves the highest scores across all metrics, demonstrating superior ability to extract and analyze features from face images.

Q: Can you describe his hairstyle? 

VILA1.5: The man in the image has a messy, unkempt hairstyle with his hair sticking up in all directions. score:4

JanusFlow: The person has a messy, spiky hairstyle with a lot of volume and texture. The hair is light brown and appears to be somewhat unkempt. score:8

UniF²ace: Certainly! He has brown hair that is thick and wavy, styled in a slightly tousled manner. His hairstyle also includes sideburns that complement the overall look. score:9

Q: Is she wearing any earrings? 

InternVL2.5: The image is not clear enough to determine if she is wearing any earrings. score:3

Show-o: Yes, the woman is wearing earrings. score:6

UniF²ace: Yes, she is wearing earrings, which add to her stylish appearance. score:7

Figure 6. Comparison of visual question-answering results and GPT-4o-based scores.

in the top (the closest to the prediction head) and bottom layers. For sequence-level MoEs, face and CLIP experts are more frequently activated in layers closer to the top, indicating that deeper layers benefit from face and image embeddings to better analyze face images. Notably, activation patterns in the understanding group differ entirely from the generation group, highlighting the effectiveness of our group-based strategy.

4.4. Ablation Studies

Coefficient in Dual Discrete Diffusion. The score-matching loss in dual discrete diffusion is approximately $200 \times$ greater than the masked generative loss, making the selection of weight coefficients α critical. We experiment with different coefficients for comparison, as shown in Tab. 3. To demonstrate the effectiveness of the D3Diff loss, we compare it with using only the masked generative loss or score loss individually. The results show that D3Diff loss achieves the best performance on the generation task. No-

Loss Type	Weight α	VQAScore-CF5 \uparrow	VQAScore-LV \uparrow	FID \downarrow	VLM-score \uparrow
D3Diff	0.1	<u>0.887</u>	<u>0.673</u>	<u>68.903</u>	86.378
	0.01	0.894	0.679	66.005	88.049
	0.001	0.884	0.668	72.736	89.220
Only Mask	0	0.879	0.661	77.463	85.993
Only Score	0.01	0.886	0.670	69.694	87.951

Table 3. Performance comparison with different loss. Considering all metrics, the optimal result is achieved with $\alpha = 0.01$ in D3Diff. **Bold:** Best performance. Underlined: Second best performance.

Token MoE	Sequence MoE	Generation			Understanding	
		VQAScore \uparrow	FID \downarrow	VLM-score \uparrow	Desc \uparrow	Conv \uparrow
\times	\times	0.878	72.877	84.432	4.988	6.031
\checkmark	\times	0.887	<u>67.415</u>	<u>87.917</u>	5.678	<u>6.495</u>
\times	\checkmark	0.889	69.312	86.790	<u>5.864</u>	6.247
\checkmark	\checkmark	0.894	66.005	88.049	6.023	6.532

Table 4. Performance impact of token-level and sequence-level MoE in UniF²ace through ablation study. Both MoEs contribute significant performance improvements.

tably, using only score loss outperforms only masked generative loss, supporting our theory proof in **Appendix D**.

Token and Sequence Level MoEs. To verify the effectiveness of the token-level and sequence-level MoE individually, we conducted a series of ablation experiments, as shown in Tab. 4. We separately evaluate metrics for generation and understanding tasks under different experimental settings. The VQAScore is assessed using CLIP-FlanT5-11B, while the understanding tasks are evaluated with GPT-4o. The results show that token-level and sequence-level MoE outperform the baseline on different tasks, while their combination achieves the best performance. This underscores the efficacy of our design in enhancing the model’s ability to extract and analyze facial features.

5. Conclusion

This paper introduces UniF²ace, the first unified multimodal model (UMM) designed for fine-grained face understanding and generation. The model bridges the gap between score-based models and masked generative models in discrete diffusion, while leveraging token-level

and sequence-level mixture-of-experts (MoE) to sparsify the model. Extensive experiments show that UniF²ace outperforms existing UMMs and even surpasses larger generation-only or understanding-only models. This underscores the potential of our improvements to guide future research in specialized applications of UMM. Additionally, we constructed a face-text aligned dataset, UniF²ace-130K, to further advance multimodal research in the community.

References

- [1] Josh Achiam, Steven Adler, Sandhini Agarwal, Lama Ahmad, Ilge Akkaya, Florencia Leoni Aleman, Diogo Almeida, Janko Altenschmidt, Sam Altman, Shyamal Anadkat, et al. Gpt-4 technical report. *arXiv preprint arXiv:2303.08774*, 2023. 2, 4
- [2] Fan Bao, Shen Nie, Kaiwen Xue, Chongxuan Li, Shi Pu, Yaole Wang, Gang Yue, Yue Cao, Hang Su, and Jun Zhu. One transformer fits all distributions in multi-modal diffusion at scale. In *International Conference on Machine Learning*, pages 1692–1717. PMLR, 2023. 1
- [3] James Betker, Gabriel Goh, Li Jing, Tim Brooks, Jianfeng Wang, Linjie Li, Long Ouyang, Juntang Zhuang, Joyce Lee, Yufei Guo, et al. Improving image generation with better captions. *Computer Science*. <https://cdn.openai.com/papers/dall-e-3.pdf>, 2(3):8, 2023. 7
- [4] Andrew Campbell, Joe Benton, Valentin De Bortoli, Thomas Rainforth, George Deligiannidis, and Arnaud Doucet. A continuous time framework for discrete denoising models. *Advances in Neural Information Processing Systems*, 35: 28266–28279, 2022. 5
- [5] Huiwen Chang, Han Zhang, Lu Jiang, Ce Liu, and William T Freeman. Maskgit: Masked generative image transformer. In *Proceedings of the IEEE/CVF conference on computer vision and pattern recognition*, pages 11315–11325, 2022. 2, 5
- [6] Xiaokang Chen, Zhiyu Wu, Xingchao Liu, Zizheng Pan, Wen Liu, Zhenda Xie, Xingkai Yu, and Chong Ruan. Januspro: Unified multimodal understanding and generation with data and model scaling. *arXiv preprint arXiv:2501.17811*, 2025. 1
- [7] Zhe Chen, Weiyun Wang, Yue Cao, Yangzhou Liu, Zhangwei Gao, Erfei Cui, Jinguo Zhu, Shenglong Ye, Hao Tian, Zhaoyang Liu, et al. Expanding performance boundaries of open-source multimodal models with model, data, and test-time scaling. *arXiv preprint arXiv:2412.05271*, 2024. 2, 8
- [8] Tahar Chettaoui, Naser Damer, and Fadi Boutros. Foundation: Are foundation models ready for face recognition? *Image and Vision Computing*, page 105453, 2025. 2, 1
- [9] M Kalpana Chowdary, Tu N Nguyen, and D Jude Hemanth. Deep learning-based facial emotion recognition for human-computer interaction applications. *Neural Computing and Applications*, 35(32):23311–23328, 2023. 1
- [10] Damai Dai, Chengqi Deng, Chenggang Zhao, RX Xu, Huazuo Gao, Deli Chen, Jiashi Li, Wangding Zeng, Xingkai Yu, Yu Wu, et al. Deepseekmoe: Towards ultimate expert specialization in mixture-of-experts language models. *arXiv preprint arXiv:2401.06066*, 2024. 5, 1
- [11] Dawei Dai, Mingming Jia, Yinxiu Zhou, Hang Xing, and Chenghang Li. Face-makeup: Multimodal facial prompts for text-to-image generation. *arXiv preprint arXiv:2501.02523*, 2025. 2, 1
- [12] Kangle Deng, Gengshan Yang, Deva Ramanan, and Jun-Yan Zhu. 3d-aware conditional image synthesis. In *Proceedings of the IEEE/CVF Conference on Computer Vision and Pattern Recognition*, pages 4434–4445, 2023. 2
- [13] Xinya Du, Junru Shao, and Claire Cardie. Learning to ask: Neural question generation for reading comprehension. In *Proceedings of the 55th Annual Meeting of the Association for Computational Linguistics*. Association for Computational Linguistics, 2017. 4
- [14] Patrick Esser, Sumith Kulal, Andreas Blattmann, Rahim Entezari, Jonas Müller, Harry Saini, Yam Levi, Dominik Lorenz, Axel Sauer, Frederic Boesel, et al. Scaling rectified flow transformers for high-resolution image synthesis. In *Forty-first international conference on machine learning*, 2024. 2, 7
- [15] Samira Hazmoune and Fateh Bougamouza. Using transformers for multimodal emotion recognition: Taxonomies and state of the art review. *Engineering Applications of Artificial Intelligence*, 133:108339, 2024. 1
- [16] Ziqi Huang, Kelvin CK Chan, Yuming Jiang, and Ziwei Liu. Collaborative diffusion for multi-modal face generation and editing. In *Proceedings of the IEEE/CVF conference on computer vision and pattern recognition*, pages 6080–6090, 2023. 2, 1
- [17] Aaron Hurst, Adam Lerer, Adam P Goucher, Adam Perelman, Aditya Ramesh, Aidan Clark, AJ Ostrow, Akila Welihinda, Alan Hayes, Alec Radford, et al. Gpt-4o system card. *arXiv preprint arXiv:2410.21276*, 2024. 2, 3, 6
- [18] Peng Jin, Bo Zhu, Li Yuan, and Shuicheng Yan. Moe++: Accelerating mixture-of-experts methods with zero-computation experts. *arXiv preprint arXiv:2410.07348*, 2024. 5
- [19] Tero Karras. A style-based generator architecture for generative adversarial networks. *arXiv preprint arXiv:1812.04948*, 2019. 3
- [20] Jihyun Kim, Changjae Oh, Hoseok Do, Soohyun Kim, and Kwanghoon Sohn. Diffusion-driven gan inversion for multi-modal face image generation. In *Proceedings of the IEEE/CVF Conference on Computer Vision and Pattern Recognition*, pages 10403–10412, 2024. 2, 1
- [21] Minchul Kim, Feng Liu, Anil Jain, and Xiaoming Liu. Dc-face: Synthetic face generation with dual condition diffusion model. In *Proceedings of the IEEE/CVF conference on computer vision and pattern recognition*, pages 12715–12725, 2023. 2
- [22] Bokyeung Lee, Hyunuk Shin, Bonhwa Ku, and Hanseok Ko. Frame level emotion guided dynamic facial expression recognition with emotion grouping. In *Proceedings of the IEEE/CVF conference on computer vision and pattern recognition*, pages 5681–5691, 2023. 1

- [23] Shufan Li, Konstantinos Kallidromitis, Akash Gokul, Zichun Liao, Yusuke Kato, Kazuki Kozuka, and Aditya Grover. Omniflow: Any-to-any generation with multi-modal rectified flows. *arXiv preprint arXiv:2412.01169*, 2024. 1, 6, 7, 8
- [24] Yifan Li, Anh Dao, Wentao Bao, Zhen Tan, Tianlong Chen, Huan Liu, and Yu Kong. Facial affective behavior analysis with instruction tuning. In *European Conference on Computer Vision*, pages 165–186. Springer, 2024. 2
- [25] Yanwei Li, Yuechen Zhang, Chengyao Wang, Zhisheng Zhong, Yixin Chen, Ruihang Chu, Shaoteng Liu, and Jiaya Jia. Mini-gemini: Mining the potential of multi-modality vision language models. *arXiv preprint arXiv:2403.18814*, 2024. 1
- [26] Zijie Li, Henry Li, Yichun Shi, Amir Barati Farimani, Yuval Kluger, Linjie Yang, and Peng Wang. Dual diffusion for unified image generation and understanding. *arXiv preprint arXiv:2501.00289*, 2024. 1
- [27] Bin Lin, Zhenyu Tang, Yang Ye, Jiayi Cui, Bin Zhu, Peng Jin, Jinfa Huang, Junwu Zhang, Yatian Pang, Munan Ning, et al. Moe-llava: Mixture of experts for large vision-language models. *arXiv preprint arXiv:2401.15947*, 2024. 1
- [28] Ji Lin, Hongxu Yin, Wei Ping, Yao Lu, Pavlo Molchanov, Andrew Tao, Huizi Mao, Jan Kautz, Mohammad Shoeybi, and Song Han. Vila: On pre-training for visual language models, 2023. 8
- [29] Aixin Liu, Bei Feng, Bing Xue, Bingxuan Wang, Bochao Wu, Chengda Lu, Chenggang Zhao, Chengqi Deng, Chenyu Zhang, Chong Ruan, et al. Deepseek-v3 technical report. *arXiv preprint arXiv:2412.19437*, 2024. 6
- [30] Haotian Liu, Chunyuan Li, Qingyang Wu, and Yong Jae Lee. Visual instruction tuning. *Advances in neural information processing systems*, 36:34892–34916, 2023. 6
- [31] Haotian Liu, Chunyuan Li, Yuheng Li, and Yong Jae Lee. Improved baselines with visual instruction tuning. In *Proceedings of the IEEE/CVF Conference on Computer Vision and Pattern Recognition*, pages 26296–26306, 2024. 2, 8
- [32] Haotian Liu, Chunyuan Li, Qingyang Wu, and Yong Jae Lee. Visual instruction tuning. *Advances in neural information processing systems*, 36, 2024. 3, 4, 6
- [33] Jiayi Liu. Chatgpt: Perspectives from human–computer interaction and psychology. *Frontiers in Artificial Intelligence*, 7:1418869, 2024. 1
- [34] Aaron Lou, Chenlin Meng, and Stefano Ermon. Discrete diffusion modeling by estimating the ratios of the data distribution. *arXiv preprint arXiv:2310.16834*, 2023. 5, 2
- [35] Aaron Lou, Chenlin Meng, and Stefano Ermon. Discrete diffusion modeling by estimating the ratios of the data distribution. In *Forty-first International Conference on Machine Learning*, 2024. 4
- [36] Yiyang Ma, Xingchao Liu, Xiaokang Chen, Wen Liu, Chengyue Wu, Zhiyu Wu, Zizheng Pan, Zhenda Xie, Haowei Zhang, Liang Zhao, et al. Janusflow: Harmonizing autoregression and rectified flow for unified multimodal understanding and generation. *arXiv preprint arXiv:2411.07975*, 2024. 1, 2, 7, 8
- [37] Andrew Melnik, Maksim Miasayedzenkau, Dzianis Makaravets, Dzianis Pirshtuk, Eren Akbulut, Dennis Holzmann, Tarek Renusch, Gustav Reichert, and Helge Ritter. Face generation and editing with stylegan: A survey. *IEEE Transactions on pattern analysis and machine intelligence*, 46(5): 3557–3576, 2024. 1
- [38] Pietro Melzi, Christian Rathgeb, Ruben Tolosana, Ruben Vera-Rodriguez, Dominik Lawatsch, Florian Domin, and Maxim Schaubert. Gandifface: Controllable generation of synthetic datasets for face recognition with realistic variations. In *Proceedings of the IEEE/CVF International Conference on Computer Vision*, pages 3086–3095, 2023. 2
- [39] Chenlin Meng, Kristy Choi, Jiaming Song, and Stefano Ermon. Concrete score matching: Generalized score matching for discrete data. *Advances in Neural Information Processing Systems*, 35:34532–34545, 2022. 2
- [40] Takeru Miyato, Shin-ichi Maeda, Masanori Koyama, and Shin Ishii. Virtual adversarial training: a regularization method for supervised and semi-supervised learning. *IEEE transactions on pattern analysis and machine intelligence*, 41(8):1979–1993, 2018. 1
- [41] Nithin Gopalakrishnan Nair, Wele Gedara Chaminda Bandara, and Vishal M Patel. Unite and conquer: Plug & play multi-modal synthesis using diffusion models. In *Proceedings of the IEEE/CVF Conference on Computer Vision and Pattern Recognition*, pages 6070–6079, 2023. 2
- [42] Alex Nichol, Prafulla Dhariwal, Aditya Ramesh, Pranav Shyam, Pamela Mishkin, Bob McGrew, Ilya Sutskever, and Mark Chen. Glide: Towards photorealistic image generation and editing with text-guided diffusion models. *arXiv preprint arXiv:2112.10741*, 2021. 1
- [43] Dustin Podell, Zion English, Kyle Lacey, Andreas Blattmann, Tim Dockhorn, Jonas Müller, Joe Penna, and Robin Rombach. Sdxl: Improving latent diffusion models for high-resolution image synthesis. *arXiv preprint arXiv:2307.01952*, 2023. 6, 7
- [44] Liao Qu, Huichao Zhang, Yiheng Liu, Xu Wang, Yi Jiang, Yiming Gao, Hu Ye, Daniel K Du, Zehuan Yuan, and Xinglong Wu. Tokenflow: Unified image tokenizer for multimodal understanding and generation. *arXiv preprint arXiv:2412.03069*, 2024. 2, 6, 7, 8
- [45] Alec Radford, Jong Wook Kim, Chris Hallacy, Aditya Ramesh, Gabriel Goh, Sandhini Agarwal, Girish Sastry, Amanda Askell, Pamela Mishkin, Jack Clark, et al. Learning transferable visual models from natural language supervision. In *International conference on machine learning*, pages 8748–8763. PMLR, 2021. 3, 6
- [46] Ahmed Roshdy, Abdullah Karar, Samer Al Kork, Taha Beyrouthy, and Amine Nait-ali. Advancements in eeg emotion recognition: Leveraging multi-modal database integration. *Applied Sciences*, 14(6):2487, 2024. 1
- [47] Subham Sekhar Sahoo, Marianne Arriola, Yair Schiff, Aaron Gokaslan, Edgar Marroquin, Justin T Chiu, Alexander Rush, and Volodymyr Kuleshov. Simple and effective masked diffusion language models. *arXiv preprint arXiv:2406.07524*, 2024. 5
- [48] Jiaxin Shi, Kehang Han, Zhe Wang, Arnaud Doucet, and Michalis Titsias. Simplified and generalized masked diffusion for discrete data. *Advances in Neural Information Processing Systems*, 37:103131–103167, 2025. 5

- [49] Weijia Shi, Xiaochuang Han, Chunting Zhou, Weixin Liang, Xi Victoria Lin, Luke Zettlemoyer, and Lili Yu. Llamafusion: Adapting pretrained language models for multimodal generation. *arXiv preprint arXiv:2412.15188*, 2024. 1
- [50] Jascha Sohl-Dickstein, Eric Weiss, Niru Maheswaranathan, and Surya Ganguli. Deep unsupervised learning using nonequilibrium thermodynamics. In *International conference on machine learning*, pages 2256–2265. pmlr, 2015. 2
- [51] S Srinivasan, R Raja, C Jehan, S Murugan, C Srinivasan, and M Muthulekshmi. Iot-enabled facial recognition for smart hospitality for contactless guest services and identity verification. In *2024 11th International Conference on Reliability, Infocom Technologies and Optimization (Trends and Future Directions)(ICRITO)*, pages 1–6. IEEE, 2024. 1
- [52] Haomiao Sun, Mingjie He, Tianheng Lian, Hu Han, and Shiguang Shan. Face-mllm: A large face perception model. *arXiv preprint arXiv:2410.20717*, 2024. 2, 1
- [53] Peize Sun, Yi Jiang, Shoufa Chen, Shilong Zhang, Bingyue Peng, Ping Luo, and Zehuan Yuan. Autoregressive model beats diffusion: Llama for scalable image generation. *arXiv preprint arXiv:2406.06525*, 2024. 2, 7
- [54] Chameleon Team. Chameleon: Mixed-modal early-fusion foundation models. *arXiv preprint arXiv:2405.09818*, 2024. 1
- [55] Gemini Team, Rohan Anil, Sebastian Borgeaud, Jean-Baptiste Alayrac, Jiahui Yu, Radu Soricut, Johan Schalkwyk, Andrew M Dai, Anja Hauth, Katie Millican, et al. Gemini: a family of highly capable multimodal models. *arXiv preprint arXiv:2312.11805*, 2023. 2
- [56] Hugo Touvron, Thibaut Lavril, Gautier Izacard, Xavier Martinet, Marie-Anne Lachaux, Timothée Lacroix, Baptiste Rozière, Naman Goyal, Eric Hambro, Faisal Azhar, et al. Llama: Open and efficient foundation language models. *arXiv preprint arXiv:2302.13971*, 2023. 1
- [57] Ashish Vaswani, Noam Shazeer, Niki Parmar, Jakob Uszkoreit, Llion Jones, Aidan N Gomez, Lukasz Kaiser, and Illia Polosukhin. Attention is all you need. *Advances in neural information processing systems*, 30, 2017. 1
- [58] Hanyang Wang, Bo Li, Shuang Wu, Siyuan Shen, Feng Liu, Shouhong Ding, and Aimin Zhou. Rethinking the learning paradigm for dynamic facial expression recognition. In *Proceedings of the IEEE/CVF conference on computer vision and pattern recognition*, pages 17958–17968, 2023. 1
- [59] Peng Wang, Shuai Bai, Sinan Tan, Shijie Wang, Zhihao Fan, Jinze Bai, Keqin Chen, Xuejing Liu, Jialin Wang, Wenbin Ge, et al. Qwen2-vl: Enhancing vision-language model’s perception of the world at any resolution. *arXiv preprint arXiv:2409.12191*, 2024. 2, 7, 8
- [60] Qixun Wang, Xu Bai, Haofan Wang, Zekui Qin, Anthony Chen, Huaxia Li, Xu Tang, and Yao Hu. Instantid: Zero-shot identity-preserving generation in seconds. *arXiv preprint arXiv:2401.07519*, 2024. 2, 1
- [61] Weilun Wang, Jianmin Bao, Wengang Zhou, Dongdong Chen, Dong Chen, Lu Yuan, and Houqiang Li. Semantic image synthesis via diffusion models. *arXiv preprint arXiv:2207.00050*, 2022. 2
- [62] Xinlong Wang, Xiaosong Zhang, Zhengxiong Luo, Quan Sun, Yufeng Cui, Jinsheng Wang, Fan Zhang, Yueze Wang, Zhen Li, Qiying Yu, et al. Emu3: Next-token prediction is all you need. *arXiv preprint arXiv:2409.18869*, 2024. 1
- [63] Junfeng Wu, Yi Jiang, Chuofan Ma, Yuliang Liu, Hengshuang Zhao, Zehuan Yuan, Song Bai, and Xiang Bai. Liquid: Language models are scalable multi-modal generators. *arXiv preprint arXiv:2412.04332*, 2024. 1
- [64] Shengqiong Wu, Hao Fei, Leigang Qu, Wei Ji, and Tat-Seng Chua. Next-gpt: Any-to-any multimodal llm. In *Forty-first International Conference on Machine Learning*, 2024. 1
- [65] Yecheng Wu, Zhuoyang Zhang, Junyu Chen, Haotian Tang, Dacheng Li, Yunhao Fang, Ligeng Zhu, Enze Xie, Hongxu Yin, Li Yi, et al. Vila-u: a unified foundation model integrating visual understanding and generation. *arXiv preprint arXiv:2409.04429*, 2024. 7, 1
- [66] Weihao Xia, Yujiu Yang, Jing-Hao Xue, and Baoyuan Wu. Tedigan: Text-guided diverse face image generation and manipulation. In *IEEE Conference on Computer Vision and Pattern Recognition (CVPR)*, 2021. 3
- [67] Jinheng Xie, Weijia Mao, Zechen Bai, David Junhao Zhang, Weihao Wang, Kevin Qinghong Lin, Yuchao Gu, Zhijie Chen, Zhenheng Yang, and Mike Zheng Shou. Show-o: One single transformer to unify multimodal understanding and generation. *arXiv preprint arXiv:2408.12528*, 2024. 1, 2, 4, 5, 6, 7, 8, 3
- [68] Bohao Xing, Zitong Yu, Xin Liu, Kaishen Yuan, Qilang Ye, Weicheng Xie, Huanjing Yue, Jingyu Yang, and Heikki Kälviäinen. Emo-llama: Enhancing facial emotion understanding with instruction tuning. *arXiv preprint arXiv:2408.11424*, 2024. 2, 1
- [69] Xingqian Xu, Zhangyang Wang, Gong Zhang, Kai Wang, and Humphrey Shi. Versatile diffusion: Text, images and variations all in one diffusion model. In *Proceedings of the IEEE/CVF International Conference on Computer Vision*, pages 7754–7765, 2023. 1
- [70] Zhipei Xu, Xuanyu Zhang, Runyi Li, Zecheng Tang, Qing Huang, and Jian Zhang. Fakeshield: Explainable image forgery detection and localization via multi-modal large language models. *arXiv preprint arXiv:2410.02761*, 2024. 2
- [71] Yichao Yan, Zanwei Zhou, Zi Wang, Jingnan Gao, and Xiaokang Yang. Dialoguenerf: Towards realistic avatar face-to-face conversation video generation. *Visual Intelligence*, 2(1):24, 2024. 2
- [72] Qu Yang, Mang Ye, and Bo Du. Emollm: Multimodal emotional understanding meets large language models. *arXiv preprint arXiv:2406.16442*, 2024. 2
- [73] Lijun Yu, José Lezama, Nitesh B Gundavarapu, Luca Versari, Kihyuk Sohn, David Minnen, Yong Cheng, Vignesh Birodkar, Agrim Gupta, Xiuye Gu, et al. Language model beats diffusion–tokenizer is key to visual generation. *arXiv preprint arXiv:2310.05737*, 2023. 6, 1
- [74] Fengda Zhang, Qianpei He, Kun Kuang, Jiashuo Liu, Long Chen, Chao Wu, Jun Xiao, and Hanwang Zhang. Distributionally generative augmentation for fair facial attribute classification. In *Proceedings of the IEEE/CVF Conference on Computer Vision and Pattern Recognition*, pages 22797–22808, 2024. 1
- [75] Zengqun Zhao, Yu Cao, Shaogang Gong, and Ioannis Patras. Enhancing zero-shot facial expression recognition by

- llm knowledge transfer. *arXiv preprint arXiv:2405.19100*, 2024. [1](#)
- [76] Yinglin Zheng, Hao Yang, Ting Zhang, Jianmin Bao, Dongdong Chen, Yangyu Huang, Lu Yuan, Dong Chen, Ming Zeng, and Fang Wen. General facial representation learning in a visual-linguistic manner. In *Proceedings of the IEEE/CVF conference on computer vision and pattern recognition*, pages 18697–18709, 2022. [2](#)
- [77] Chunting Zhou, Lili Yu, Arun Babu, Kushal Tirumala, Michihiro Yasunaga, Leonid Shamis, Jacob Kahn, Xuezhe Ma, Luke Zettlemoyer, and Omer Levy. Transfusion: Predict the next token and diffuse images with one multi-modal model. *arXiv preprint arXiv:2408.11039*, 2024. [1](#), [4](#)
- [78] Hao Zhu, Wayne Wu, Wentao Zhu, Liming Jiang, Siwei Tang, Li Zhang, Ziwei Liu, and Chen Change Loy. CelebV-HQ: A large-scale video facial attributes dataset. In *ECCV*, 2022. [2](#), [3](#)

UniF²ace: Fine-grained Face Understanding and Generation with Unified Multimodal Models

Supplementary Material

1. Appendix A: Related Works

Unified Multimodal Models. Recent works [6, 26, 36, 62, 63] in image understanding and generation have primarily focused on unified multimodal models (UMMs). Early approaches [25, 64] often integrated external decoders of diffusion models (DMs) with text autoregressive models (ARMs). Inspired by next-token prediction tasks, they proposed using a single Transformer [57] model to unify understanding and generation [65]. For instance, Janus-Pro [6] decouples the visual encoder into specialized tokenizers for separate handling of understanding and generation tasks. Chameleon [54] and Emu3 [62] employ an ARM to simultaneously manage both tasks, highlighting the advantages of autoregressive models in multitask settings. Additionally, Transfusion [77] and Show-o [67] combine a text ARM with a visual DM, enabling seamless integration of image understanding and generation. These studies have advanced the fusion of visual and text generation models, enhancing performance on multimodal tasks. However, despite the proliferation of UMMs, their application has largely been limited to generic domain tasks, with limited exploration in fine-grained visual analysis, particularly in the face domain. Unlike previous UMMs that simply combine ARMs and DMs, we pioneer sparse UMMs by introducing both token-level and sequence-level Mixture of Experts (MoEs), significantly improving model performance.

Face Multimodal Models. Face multimodal models are primarily categorized into two types: face understanding models and face generation models. For understanding, early models were task-specific and lacked multimodality [22, 40, 58, 74]. Recent works [8, 52, 68, 75] leverage the reasoning capabilities of LLMs or MLLMs, often using MLLM-generated face Q&A data to fine-tune or post-train foundation models, incorporating face domain knowledge. For example, EMO-LLaMA [68] introduces facial experts to extract facial features, which are aggregated with handcrafted prompts and fed into LLaMA [56], enabling it to answer facial-related queries. For generation, recent works [11, 16, 20, 60] focus on using diffusion models to personalize face images by conditioning on textual and visual information, such as semantic masks, but avoid directly capturing fine-grained face attributes from text prompts. Despite these advances in understanding and generation separately, developing unified multimodal models (UMMs) remains a significant research challenge.

Addressing this gap can enhance cross-modal capabilities and advance progress toward Artificial General Intelligence (AGI).

2. Appendix B: Implementations Details

Our UMM backbone is based on Show-o [67]. UniF²ace utilizes discrete image tokens as input, represented by the pre-trained MAGVIT-v2 [73]. For token-level MoE, each group (generation and understanding tasks) includes one shared expert and eight routed experts, selected via a top-2 strategy. The expert structure is a single-layer MLP with the gating mechanism [10]. In sequence-level MoE, the generation group employs two copy experts, one zero expert, and one noise expert. Noise embedding is implemented using sinusoidal embedding, following [42]. The noise resampler uses a 4-layer Multi-Head Attention mechanism to map noise embeddings to the UniF²ace hidden space. For the understanding group, there are two copy experts, one CLIP expert, and one face expert. We use CLIP-ViT for image embedding and AntelopeV2 for face embedding, with the resampler configuration matching that of the noise expert. Moreover, training is divided into two stages: Stage I uses only captions for generation and understanding tasks, while Stage II incorporates VQAs into the understanding task. This pipeline transitions the model from general image feature understanding to fine-grained feature capture. Both stages are trained on 8 NVIDIA A100 (80GB) GPUs, optimized using AdamW with a weight decay of 0.01, 5K warm-up steps, and an initial learning rate of $5e-5$ with cosine scheduling. The total batch size is 600 for Stage I and 480 for Stage II, with 20K steps for Stage I and 40K steps for Stage II. In the inference process of UniF²ace, following the computation method in [27], we compute the maximum and minimum activation parameters for UniF²ace under the Top-2 strategy due to the different number of parameters included between different experts in the sequence-level MoE. The total number of parameters for UniF²ace is 1.84B, the maximum activation parameter is about 1.63B, and the minimum activation parameter is about 1.42B. The average number of activation parameters tested in the UniF²ace-130K test dataset is 1.47B.

3. Appendix C: Absorbing-state Case with Independence between Tokens.

The absorbing-state case means that for any single token x with possible values in $\mathcal{X} = \{1, \dots, N\}$, the transition

matrix is

$$Q^{\text{absorb}} = \begin{bmatrix} -1 & 0 & \cdots & 0 & 1 \\ 0 & -1 & \cdots & 0 & 1 \\ \vdots & \vdots & \ddots & \vdots & \vdots \\ 0 & 0 & \cdots & -1 & 1 \\ 0 & 0 & \cdots & 0 & 0 \end{bmatrix}.$$

The reverse transition rate matrix of the reverse process from state x_t to state \hat{x}_t is

$$\tilde{Q}_t(x_t, \hat{x}_t) = \begin{cases} \frac{p_t(\hat{x}_t)}{p_t(x_t)} Q_t(\hat{x}_t, x_t), & \hat{x}_t \neq x_t \\ -\sum_{k \neq x_t} \tilde{Q}_t(x_t, k), & \hat{x}_t = x_t \end{cases}.$$

As $Q_t(\hat{x}_t, x_t)$ is known, it is sufficient to estimate the concrete score $\frac{p_t(\hat{x}_t)}{p_t(x_t)}$ by a score network $s_\theta(x_t, t) \approx \left[\frac{p_t(\hat{x}_t)}{p_t(x_t)} \right]_{\hat{x}_t \in \mathcal{X}}$. Score based discrete diffusion model is an effective objective to train the score network [34, 39]. Specifically, the score function in multidimensional discrete space is

$$\begin{aligned} s_\theta(\mathbf{x}_t, t)_{\hat{x}_t} &= s_\theta(x_t^1 \dots x_t^i \dots x_t^d, t) [i, \hat{x}_t^i] \\ &\approx \frac{p_t(x_t^1 \dots \hat{x}_t^i \dots x_t^d)}{p_t(x_t^1 \dots x_t^i \dots x_t^d)}, \end{aligned}$$

and accordingly,

$$\begin{aligned} \tilde{Q}_t(x_t^1 \dots x_t^i \dots x_t^d, x_t^1 \dots \hat{x}_t^i \dots x_t^d) \\ \approx Q_t(\hat{x}_t^i, x_t^i) s_\theta(x_t^1 \dots x_t^i \dots x_t^d, t) [i, \hat{x}_t^i]. \end{aligned}$$

4. Appendix D: Relationship Between Score Loss and Masked Generative Loss.

To prove that our score loss (loss (1)) provides a tighter upper bound, we first introduce these two losses.

- (1) $\mathcal{L}_1 = \mathcal{L}_{\text{score}}(x_0) + D_{KL}(p_{T|0}(\cdot | x_0) \| p_{\text{base}})$, where $\mathcal{L}_{\text{score}}(x_0)$ is the diffusion weighted denoising score entropy for data point x_0 , and $s_\theta = \frac{p_\theta(x_0|x_t)}{p(x_t|x_0)}$

$$\begin{aligned} \mathcal{L}_{\text{score}}(x_0) &= \int_0^T \mathbb{E}_{x_t \sim p_{t|0}(\cdot | x_0)} \sum_{y \neq x_t} Q_t(x_t, y) \left(s_\theta(x_t, t)_y \right. \\ &\quad \left. - \frac{p_{t|0}(y | x_0)}{p_{t|0}(x_t | x_0)} \log s_\theta(x_t, t)_y + K \left(\frac{p_{t|0}(y | x_0)}{p_{t|0}(x_t | x_0)} \right) \right) dt. \end{aligned}$$

- (2) $\mathcal{L}_2 = -\sum_{t=1}^T \mathbb{E}_{q(\mathbf{x}_0)q(\mathbf{x}_t|\mathbf{x}_0)} [\log p_\theta(\mathbf{x}_0 | \mathbf{x}_t)] - C$, where where $C = C_1 + C_2$. The constants C_1 and C_2 are [67]:

$$\begin{aligned} C_1 &= \mathbb{E}_{q(\mathbf{x}_{0:T})} \left[-\sum_{t=1}^T \log q(\mathbf{x}_t | \mathbf{x}_{t-1}) + \underbrace{\log p(\mathbf{x}_T)}_{\text{Note that } p(\mathbf{x}_T)=q(\mathbf{x}_T)} \right] \\ &= \mathbb{E}_{q(\mathbf{x}_{0:T})} \left[-\sum_{t=1}^T \log q(\mathbf{x}_t, \mathbf{x}_{t-1}) + \sum_{t=0}^T \log q(\mathbf{x}_t) \right], \end{aligned} \quad (15)$$

$$\begin{aligned} C_2 &= \mathbb{E}_{q(\mathbf{x}_{0:T})} \left[\sum_{t=1}^T \log q(\mathbf{x}_{t-1} | \mathbf{x}_t) \right] \\ &\quad - \mathbb{E}_{q(\mathbf{x}_{0:T})} \left[\sum_{t=1}^T \sum_{\tilde{\mathbf{x}}_0} q(\tilde{\mathbf{x}}_0 | \mathbf{x}_{t-1}) \log q(\tilde{\mathbf{x}}_0 | \mathbf{x}_t) \right] \\ &= \mathbb{E}_{q(\mathbf{x}_{0:T})} \left[\sum_{t=1}^T \log q(\mathbf{x}_t, \mathbf{x}_{t-1}) - \sum_{t=1}^T \log q(\mathbf{x}_t) \right] \\ &\quad - \sum_{t=1}^T \mathbb{E}_{q(\mathbf{x}_{0:T})q(\tilde{\mathbf{x}}_0|\mathbf{x}_{t-1})} [\log q(\tilde{\mathbf{x}}_0 | \mathbf{x}_t)]. \end{aligned}$$

$$C_1 + C_2 = \mathbb{E}_{q(\mathbf{x}_{0:T})} \left[\log q(\mathbf{x}_0) - \sum_{t=1}^T \log q(\mathbf{x}_0 | \mathbf{x}_t) \right].$$

From the derivation of [34, 67], both losses are expanded in the classic way of likelihood function (as equation (a)) by Jensen inequality.

$$\begin{aligned} &\log p_0^\theta(x_0) \\ &= \mathbb{E}_{q(\mathbf{x}_0)} \left[\log \int p_\theta(\mathbf{x}_0, \mathbf{x}_1 \dots \mathbf{x}_T) d\mathbf{x}_1 \dots d\mathbf{x}_T \right] \\ &= \mathbb{E}_{q(\mathbf{x}_0)} \left\{ \log \mathbb{E}_{q(\mathbf{x}_{1:T}|\mathbf{x}_0)} \left[\frac{p_\theta(\mathbf{x}_{0:T-1} | \mathbf{x}_T)}{q(\mathbf{x}_{1:T} | \mathbf{x}_0)} p(\mathbf{x}_T) \right] \right\} \\ &\stackrel{(a)}{\geq} \mathbb{E}_{q(\mathbf{x}_0)q(\mathbf{x}_{1:T}|\mathbf{x}_0)} \left[\log \frac{p_\theta(\mathbf{x}_{0:T-1} | \mathbf{x}_T)}{q(\mathbf{x}_{1:T} | \mathbf{x}_0)} + \log p(\mathbf{x}_T) \right] \end{aligned} \quad (16)$$

Let L be the posterior probability $L = \log p_0^\theta(x_0)$, and $K = \mathbb{E}_{q(\mathbf{x}_0)q(\mathbf{x}_{1:T}|\mathbf{x}_0)} \left[\log \frac{p_\theta(\mathbf{x}_{0:T-1} | \mathbf{x}_T)}{q(\mathbf{x}_{1:T} | \mathbf{x}_0)} + \log p(\mathbf{x}_T) \right]$, then $L \geq K$.

Analysis of \mathcal{L}_1 . Inspired by [50], we then illustrate that $K = -\mathcal{L}_1$. Assume that q is the forward transition, and p is the transition of reverse process, $p(x_T) \approx q(x_T)$. As [50] states, the term K is equal to the following formula strictly,

$$\begin{aligned} K &= -\sum_{t=2}^T \int dx_0 dx_t q(x_0, x_t) \\ &\quad \cdot KL(q(x_{t-1} | x_t, x_0) \| p(x_{t-1} | x_t)) \\ &\quad + H_q(x_T | x_0) - H_q(x_1 | x_0) - H_p(x_T) \end{aligned}$$

Since

$$\begin{aligned} &H_q(x_T | x_0) - H_p(x_T) \\ &= \int_{x_T} \int_{x_0} q(x_T | x_0) q(x_0) \log q(x_T | x_0) dx_0 dx_T \\ &\quad - \int_{x_T} \int_{x_0} q(x_T | x_0) q(x_0) dx_0 \log p(x_T) dx_T \\ &= \int_{x_T} \int_{x_0} q(x_T | x_0) q(x_0) \log \frac{q(x_T | x_0)}{p(x_T)} dx_0 dx_T \\ &= \mathbb{E}_{p_{\text{data}}(x_0)} [KL(q(x_T | x_0) \| p(x_T))] \end{aligned} \quad (17)$$

In addition,

$$H_q(x_1 | x_0) = \mathbb{E}_{p_{\text{data}}} \mathbb{E}_{q(x_1|x_0)} [\log p_{0|1}(x_0 | x_1)]$$

Then K is equivalent to $-\mathbb{E}_{x_T \sim p_{T|0}(\cdot | x_0)} [D_{\text{KL}}(\mathbb{P}_{x_0}(\cdot | x_T) \|\mathbb{P}^\theta(\cdot | x_T))]$ $- D_{\text{KL}}(p_{T|0}(\cdot | x_0) \|\pi)$, or to say, $K = -(\mathcal{L}_{\text{score}} + D_{\text{KL}}(p_{T|0}(\cdot | x_0) \|\pi))$, which is our loss. This is to say that $K = \mathcal{L}_1$ strictly.

Analysis of \mathcal{L}_2 . The proof of \mathcal{L}_2 performs a second scaling based on (a) (still using Jensen's inequality), see (b).

$$\begin{aligned} K &= \mathbb{E}_{q(\mathbf{x}_0)q(\mathbf{x}_{1:T}|\mathbf{x}_0)} \left[\log \frac{p_\theta(\mathbf{x}_{0:T-1} | \mathbf{x}_T)}{q(\mathbf{x}_{1:T} | \mathbf{x}_0)} + \log p(\mathbf{x}_T) \right] \\ &= \mathbb{E}_{q(\mathbf{x}_{0:T})} \left[\sum_{t \geq 1}^T \log \frac{p_\theta(\mathbf{x}_{t-1} | \mathbf{x}_t)}{q(\mathbf{x}_t | \mathbf{x}_{t-1})} + \log p(\mathbf{x}_T) \right] \\ &= \mathbb{E}_{q(\mathbf{x}_{0:T})} \left[\sum_{t \geq 1}^T \log \sum_{\tilde{\mathbf{x}}_0} q(\mathbf{x}_{t-1} | \mathbf{x}_t, \tilde{\mathbf{x}}_0) \tilde{p}_\theta(\tilde{\mathbf{x}}_0 | \mathbf{x}_t) \right] \\ &\quad + \underbrace{\mathbb{E}_{q(\mathbf{x}_{0:T})} \left[\log p(\mathbf{x}_T) - \sum_{t \geq 1}^T \log q(\mathbf{x}_t | \mathbf{x}_{t-1}) \right]}_{C_1} \\ &= \mathbb{E}_{q(\mathbf{x}_{0:T})} \left[\sum_{t \geq 1}^T \log \sum_{\tilde{\mathbf{x}}_0} \frac{q(\tilde{\mathbf{x}}_0 | \mathbf{x}_{t-1})}{q(\tilde{\mathbf{x}}_0 | \mathbf{x}_t)} \right. \\ &\quad \left. \underbrace{\frac{q(\mathbf{x}_t | \mathbf{x}_{t-1})q(\mathbf{x}_{t-1})}{q(\mathbf{x}_{t-1} | \mathbf{x}_t)}}_{\tilde{p}_\theta(\tilde{\mathbf{x}}_0 | \mathbf{x}_t)} \right] + C_1 \\ &\stackrel{(b)}{\geq} \mathbb{E}_{q(\mathbf{x}_{0:T})} \left[\sum_{t \geq 1}^T \sum_{\tilde{\mathbf{x}}_0} q(\tilde{\mathbf{x}}_0 | \mathbf{x}_{t-1}) \right. \\ &\quad \left. \cdot \log \left(\frac{q(\mathbf{x}_{t-1} | \mathbf{x}_t)}{q(\tilde{\mathbf{x}}_0 | \mathbf{x}_t)} \tilde{p}_\theta(\tilde{\mathbf{x}}_0 | \mathbf{x}_t) \right) \right] + C_1 \\ &= \sum_{t \geq 1}^T \mathbb{E}_{q(\mathbf{x}_t, \mathbf{x}_0)} [\log \tilde{p}_\theta(\mathbf{x}_0 | \mathbf{x}_t)] + C_1 + C_2 = -\mathcal{L}_2. \end{aligned}$$

The intermediate derivation process is from [67]. Therefore,

$$\begin{aligned} L &\stackrel{(a)}{\geq} K = -\mathcal{L}_1 \stackrel{(b)}{\geq} -\mathcal{L}_2 \\ \text{i.e. } &-(\mathcal{L}_{\text{score}}(x_0) + D_{\text{KL}}(p_{T|0}(\cdot | x_0) \|\pi_{\text{base}})) \\ &\geq \sum_{t \geq 1}^T \mathbb{E}_{q(\mathbf{x}_t, \mathbf{x}_0)} [\log \tilde{p}_\theta(\mathbf{x}_0 | \mathbf{x}_t)] + C_1 + C_2. \end{aligned} \quad (18)$$

Then

$$\mathcal{L}_{\text{score}}(x_0) + D_{\text{KL}}(p_{T|0}(\cdot | x_0) \|\pi_{\text{base}})$$

$$\leq -\sum_{t=1}^T \mathbb{E}_{q(\mathbf{x}_0)q(\mathbf{x}_t|\mathbf{x}_0)} [\log p_\theta(\mathbf{x}_0 | \mathbf{x}_t)] - (C_1 + C_2).$$

Analysis of $C_1 + C_2 + D_{\text{KL}}(p_{T|0}(\cdot | x_0))$.

If $C_1 + C_2 + D_{\text{KL}}(p_{T|0}(\cdot | x_0)) \geq 0$, then we accomplish the proof that our bound is a smaller upper bound. Since $C_1 + C_2 = E_{q(x_{0:T})} [\log q(x_0) - \sum_{t=1}^T \log q(x_0|x_t)]$, $D_{\text{KL}}(p_{T|0}(\cdot | x_0)) = H_q(x_T|x_0) - H_q(x_T)$, we then we aim to simplify the following expression:

$$E_{q(x_{0:T})} \left[\log q(x_0) - \sum_{t=1}^T \log q(x_0|x_t) \right] + (H_q(x_T|x_0) - H_q(x_T)). \quad (19)$$

First, recall the definition of entropy and the conditional entropy:

$$H_q(x) = -E_{q(x)}[\log q(x)] = -\sum_x q(x) \log q(x). \quad (20)$$

$$H_q(x|y) = -E_{q(x,y)}[\log q(x|y)] = -\sum_{x,y} q(x,y) \log q(x|y). \quad (21)$$

Expanding the expectation in the given expression:

$$E_{q(x_{0:T})} \left[\log q(x_0) - \sum_{t=1}^T \log q(x_0|x_t) \right] \quad (22)$$

$$= \sum_{x_{0:T}} q(x_{0:T}) \left[\log q(x_0) - \sum_{t=1}^T \log q(x_0|x_t) \right]. \quad (23)$$

Rewriting the terms:

$$\sum_{x_{0:T}} q(x_{0:T}) \log q(x_0) = \sum_{x_0} q(x_0) \log q(x_0) = -H_q(x_0), \quad (24)$$

$$\begin{aligned} &\sum_{x_{0:T}} q(x_{0:T}) \sum_{t=1}^T \log q(x_0|x_t) \\ &= \sum_{t=1}^T \sum_{x_t} q(x_t) \sum_{x_0} q(x_0|x_t) \log q(x_0|x_t) \\ &= \sum_{t=1}^T E_{q(x_t)} [H_q(x_0|x_t)]. \end{aligned} \quad (25)$$

Thus, the first term simplifies to:

$$H_q(x_0) - \sum_{t=1}^T E_{q(x_t)} [H_q(x_0|x_t)]. \quad (26)$$

Combining these terms,

$$\begin{aligned} & H_q(x_0) - \sum_{t=1}^T E_{q(x_t)}[H_q(x_0|x_t)] + (H_q(x_T|x_0) - H_q(x_T)) \\ &= H_q(x_0) - H_q(x_T) - \sum_{t=1}^T E_{q(x_t)}[H_q(x_0|x_t)] + H_q(x_T|x_0). \end{aligned} \quad (27)$$

Using the inequality that the expectation of conditional entropy satisfies:

$$\sum_{t=1}^T E_{q(x_t)}[H_q(x_0|x_t)] \leq H_q(x_0), \quad (28)$$

Since we only consider absorbing process, x_T is fully masked at time T , thus $H(x_T) = 0$. We then conclude that the entire expression is non-negative:

$$H_q(x_0) - \sum_{t=1}^T E_{q(x_t)}[H_q(x_0|x_t)] \geq 0, \quad (29)$$

and the above formula equal to 0 holds true when for any t , x_t and x_0 are independent. Therefore, we have:

$$\mathcal{L}_{\text{score}}(x_0) \leq - \sum_{t=1}^T \mathbb{E}_{q(\mathbf{x}_0)q(\mathbf{x}_t|\mathbf{x}_0)} [\log p_\theta(\mathbf{x}_0 | \mathbf{x}_t)].$$

5. Appendix E: Implementation of the Resampler

We define a resampler $S : \mathbb{R}^h \rightarrow \mathbb{R}^{L \times D}$, where h is the length of the input vector, L is the length of the sequence and D is the hidden dimension of UniF²ace. Specifically, we define a learnable hidden latent matrix:

$$\mathbf{M}_0 \in \mathbb{R}^{L \times d}, \quad \mathbf{M}_0 = \text{LearnableParameter}$$

where d is the hidden dimension of the resampler. Its process involves:

1. Project the noise embedding $\mathbf{x} \in \mathbb{R}^h$ via

$$\mathbf{H} = \mathbf{x}\mathbf{W}_{\text{in}} \in \mathbb{R}^{1 \times d}$$

2. Iteratively refine the latent matrix through T layers, such as the l -th layer:

$$\begin{aligned} \mathbf{M}'_l &= \mathbf{M}_{l-1} + \text{MHA}(\mathbf{M}_{l-1}, \text{Concat}(\mathbf{H}, \mathbf{M}_{l-1})) \\ \mathbf{M}_l &= \mathbf{M}'_l + \text{FFN}(\mathbf{M}'_l) \end{aligned}$$

where MHA denotes the Multi-Head Attention mechanism, FFN denotes the Feed-Forward Network. In MHA, the query, key, and value are denoted as:

$$\begin{aligned} Q_l &= M_{l-1}W_Q^{(l)} \\ K_l &= [H; M_{l-1}]W_K^{(l)} \\ V_l &= [H; M_{l-1}]W_V^{(l)} \end{aligned}$$

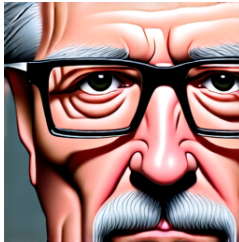
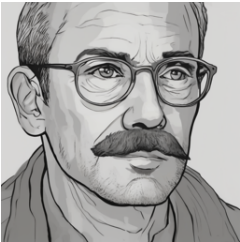
3. Project the final latent to the output space:

$$\mathbf{Y} = \text{LayerNorm}(\mathbf{M}_T\mathbf{W}_{\text{out}}) \in \mathbb{R}^{L \times D}$$

This enables adaptive fusion of input vector into sequence features through learned latent queries.

SDXL**TokenFlow****OmniFlow****Show-o****UniF²ace(Ours)**

"A male with short, slightly tousled gray hair and a distinct goatee. His face is characterized by a broad forehead and prominent cheekbones. The nose is straight and well-defined. The skin tone is warm, with natural texture and some visible lines, indicative of age and life experience."



"The image features a male with a receding hairline and short, gray hair. He has a mustache and a neatly trimmed beard. The person is wearing thin-framed eyeglasses that rest on his nose. His expression appears serious or contemplative, with closed lips and focused eyes. The lighting highlights the contours of his face, emphasizing the forehead and cheekbones. The background is slightly blurred, featuring an American flag, suggesting a formal or official setting. The overall composition conveys a sense of gravity and focus."



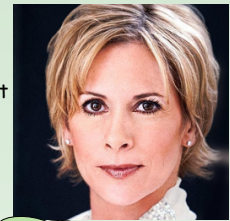
"The person in the image has a warm and friendly expression, characterized by a gentle smile that conveys happiness. They appear to be female and have light skin, with long hair partially covered by a patterned headscarf in shades of green and blue, adding elegance to their appearance. The decorative headpiece features a central red gem and dangling elements across the forehead. Their eyes are accentuated with dark eyeliner, and they have arched eyebrows that complement their facial features. The person is wearing lipstick, which enhances their smile, and they have a pointy nose. Additionally, they are wearing earrings that add a touch of sophistication. The lighting highlights the smooth texture of their skin, enhancing the natural beauty of their face."

Figure 1. More comparison of generated face images with other models.



Figure 2. More face images generated by UniF²ace

Q: Break down the elements of the image in a detailed manner.



VILA1.5: The image captures a close-up portrait of a woman, her face filling most of the frame. Her hair, a vibrant shade of **blonde**. She is adorned with a **pair of earrings**, a subtle accessory that complements her overall look. Her **gaze is directed straight** at the camera, creating a sense of connection with the viewer. The background is a stark black, providing a striking contrast to her blonde hair and **white blouse**. The image does not contain any discernible text or additional objects. The relative position of the woman in the frame and the absence of other elements give the image a minimalist aesthetic. The image is a study in contrasts - the blonde hair against the black background, the white blouse against the black background, and the woman's direct gaze against the surrounding darkness. **score:8**

Qwen2-VL: The image features a person with **short, blonde hair** styled in a neat, **straight** manner. The **hair is parted slightly off-center**, and the individual is wearing a **white, high-collared garment**. The background is plain and dark, which helps to highlight the subject. The person is **looking directly** at the camera, giving a sense of direct engagement with the viewer. The lighting is soft, evenly illuminating the subject's face and hair, without casting harsh shadows. The overall composition is simple and focused, emphasizing the subject's facial features and attire. **score:6**

LLaVA-v1.5: The image features a woman with **short blonde hair**, wearing a **white shirt** and a **necklace**. She is **looking directly** at the camera, giving a **confident** and professional appearance. The woman appears to be well-dressed and poised, possibly for a formal event or a professional setting. **score:4**

InternVL2.5: The image captures a close-up portrait of a woman with **light skin** and **short, straight blond hair**. Her hair **falls just above her shoulders**, framing her face in soft waves at the ends. Her eyes are a **light shade**, possibly hazel or **blue**, and she has a **slight smile** on her lips. She wears makeup that includes **mascara** and possibly a **neutral lipstick**, enhancing her natural features without appearing overly done. The woman's ears are adorned with **small, round earrings** that catch the light, suggesting they may be **made of a metallic or pearl-like material**. The background is not visible, focusing attention solely on the woman's face. There are no discernible texts, symbols, or other objects in the image. **score:7**

OmniFlow: a woman with **blonde hair** and **bangs**. **score:6**

JanusFlow: The image features a woman with **short, blonde hair** styled in a layered cut. Her hair is **parted to the side**, and she has a few strands framing her face. She is wearing **small, round earrings**. The background is dark, which contrasts with her **light-colored hair and clothing**. The woman is wearing a **white or light-colored top** with a **high collar**, which appears to be made of a textured or patterned fabric. **score:6**

Show-o: The image features a woman with **blonde hair** and a **white collar**, **wearing a white dress**. She is **looking directly** at the camera, her gaze steady and confident. The background is dark, providing a stark contrast to her **bright attire**. The woman's expression and pose **give the impression of a professional portrait**, possibly for a magazine or a professional setting. **score:5**

Uni²Face(Ours): The image features a female with **short, blonde hair** styled in a **layered cut with bangs**. Her hair appears **wavy**, and she has a **receding hairline**. She has a **fair complexion** and **smooth skin texture**. Her **well-groomed, arched eyebrows** frame expressive eyes that are highlighted by **long lashes**. The person has a **straight nose** and **lipstick**, contributing to her **balanced and symmetrical face**. Her expression is neutral, exuding a **calm and confident** demeanor with a **direct gaze**. She is wearing **earrings**, and her **subtle makeup** enhances her natural features beautifully. **score:9**

Figure 3. Comparison of captioning results and DeepSeeek-v3-based scores. We highlight fine-grained attributes with blue and errors in answers with red.

Step1: Prompt for generating initial captions:

User: "In the image there is a person, describe the image in a paragraph giving detailed fine-grained attributes of the person face. [Note that the output is mixed with the captions given below: xxxxx]"

Step2: Prompt for generating fine-grained captios:

User: "Please combine the face caption you just replied to and the following features into one paragraph:
Appearance: xxx, xxx, xxx, xxx.....
Action: xxx, xxx, xxx.....
Emotion: xxx

Step3: Prompt for generating fine-grained VQAs

User: You are an AI visual assistant, and you are seeing a face image. What you see are provided with a paragraph , describing the same image you are looking at. Answer all questions as you are seeing the image.

Design a conversation between you and a person asking about this photo. The answers should be in a tone that a visual AI assistant is seeing the image and answering the question.

Ask diverse questions and give corresponding answers.

Questions cover as many face attributes as possible, such as hair, nose, eyes, mouth, ears, skin, eyebrows, adornment, and so on. Only include questions that have definite answers:

- (1) one can see the content in the image that the question asks about and can answer confidently;
- (2) one can determine confidently from the image that it is not in the image.

Do not ask any question that cannot be answered confidently.

Also include closed-ended questions that are relevant to the content in the image, for example, asking whether the person in the image has earrings, asking whether is the hair of the person in the image long or short, etc. Again, do not ask about uncertain details.

Also include complex questions that are relevant to the content in the image, for example, asking about the action and emotion of the person in the image, asking to discuss about events happening in the image, etc. Again, do not ask about uncertain details.

Provide detailed answers when answering complex questions. For example, give detailed examples or reasoning steps to make the content more convincing and well-organized. You can include multiple paragraphs if necessary.

Please return the results in the following json format:

Example:

```
{"from": "human", "value": "Can you describe his eyes and eyebrows?"},
```

```
{"from": "gpt", "value": "Certainly! His eyes are deep-set and expressive, and his bushy dark eyebrows complement them well, enhancing his expressive appearance."},
```

```
{"from": "human", "value": "What color are her earrings?"},
```

```
{"from": "gpt", "value": "She wears gold earrings."},
```

Figure 4. Prompts for building dataset. The first and second prompts are to GPT-4o, while the last prompt is to GPT-4. In the first prompt, the content in "[]" is used only when the image data includes built-in captions, such as in MM-CelebA-HQ dataset.